EBSD data analysis with MATHLAB toolbox MTEX

Helmut Schaeben[1] and Ralf Hielscher[2]

[1]TU Bergakademie Freiberg, Germany
[2]Helmholtz Zentrum München, Germany

EBSD Workshop, Chemnitz, 18.–19. Mai 2009

Contents

- **Challenges of texture analysis**
- **Unique approach to texture analysis with integral or individual orientation measurements**
- **A practical application**
- **Conclusions**

Challenges of texture analysis

Objective of texture analysis

Determination of an orientation probability density function,

1. which globally or locally explains experimental "integral" pole intensity data well, or
2. which is derived from individual orientation measurements,

and its characteristics like

- harmonic (Fourier) coefficients,
- texture index,
- entropy,
- volume fractions around peaks or fibres
- ...
- ...

Orientation distribution within a single hematite crystal

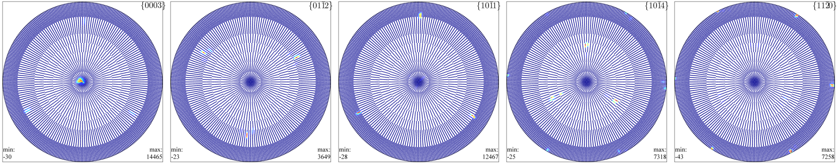

Neutron diffraction pole figure data corresponding to a grid comprising $14,616$ positions with a mean distance of 1.5 degree

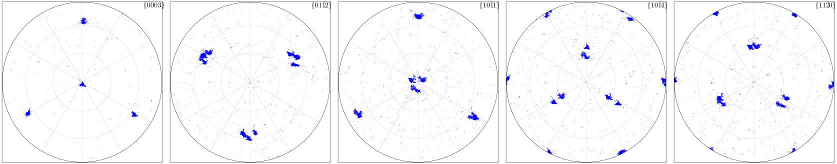

Pole point plots corresponding to a total of $69,541$ individual orientation measurements

Data courtesy Heinrich Siemes, RWTH Aachen

Comparison by numbers

Neutron	(α, β, γ)	$\int_{b(g_m;10)} f(g)dg$	$f(\alpha, \beta, \gamma)$
g_M (black)	$(155, 3, 53)$	0.45	$14,709$
g_{m_1} (blue)	$(90, 65, 59)$	0.09	675
g_{m_2} (red)	$(30, 115, 1)$	0.18	750
g_{m_3} (green)	$(150, 115, 1)$	0.09	545
sum		0.36	

EBSD	(α, β, γ)	$\int_{b(g_m;10)} f(g)dg$	$f(\alpha, \beta, \gamma)$
g_M (black)	$(100, 178, 11)$	0.45	$12,251$
g_{m_1} (blue)	$(90, 65, 59)$	0.05	699
g_{m_2} (red)	$(30, 115, 1)$	0.04	450
g_{m_3} (green)	$(150, 115, 1)$	0.33	$2,611$
sum		0.42	

Unique approach to texture analysis
with integral or individual orientation measurements

Examples of radially symmetric functions

de la Vallée Poussin kernel

$$\psi_\kappa(\omega(\boldsymbol{g}\boldsymbol{g}_0^{-1})) = \frac{B(\frac{3}{2},\frac{1}{2})}{B(\frac{3}{2},\kappa+\frac{1}{2})} \cos^{2\kappa} \frac{\omega(\boldsymbol{g}\boldsymbol{g}_0^{-1})}{2},$$

$$\mathcal{R}\psi_\kappa(\mathbf{h},\mathbf{r}) = (1+\kappa)\cos^{2\kappa} \frac{\arccos(\boldsymbol{g}_0\mathbf{h}\cdot\mathbf{r})}{2}$$

de la Vallée Poussin

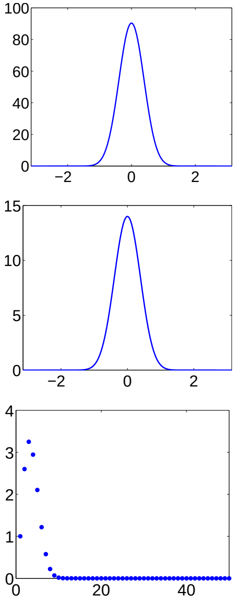

Examples of radially symmetric functions

de la Vallée Poussin kernel

$$\psi_\kappa(\omega(\boldsymbol{g}\boldsymbol{g}_0^{-1})) = \frac{B(\frac{3}{2},\frac{1}{2})}{B(\frac{3}{2},\kappa+\frac{1}{2})} \cos^{2\kappa} \frac{\omega(\boldsymbol{g}\boldsymbol{g}_0^{-1})}{2},$$

$$\mathcal{R}\psi_\kappa(\mathbf{h},\mathbf{r}) = (1+\kappa) \cos^{2\kappa} \frac{\arccos(\boldsymbol{g}_0\mathbf{h}\cdot\mathbf{r})}{2}$$

von Mises–Fisher kernel

$$\psi_\kappa(\omega(\boldsymbol{g})) = \frac{1}{\mathcal{I}_0(\kappa)-\mathcal{I}_1(\kappa)} e^{2\kappa\cos^2\frac{\omega(\boldsymbol{g})}{2}-\kappa},$$

$$\mathcal{R}\psi_\kappa(\mathbf{h},\mathbf{r}) = \frac{\mathcal{I}_0(\kappa\cos 2\angle(\mathbf{h},\mathbf{r}))}{\mathcal{I}_0(\kappa)-\mathcal{I}_1(\kappa)} e^{\frac{\kappa}{2}(\mathbf{h}\cdot\mathbf{r}-1)}$$

von Mises–Fisher

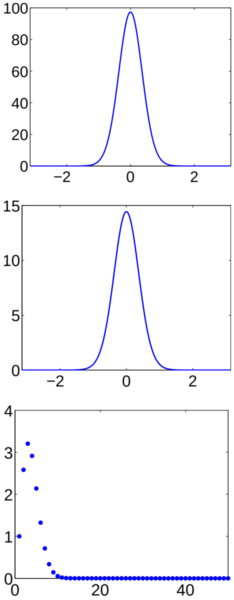

Resolution of the pdf–to–odf inversion problem

Ansatz ...

The odf is modelled as a positive linear combination

$$f(\boldsymbol{g}) = \sum_{m=1}^{M} c_m \, \psi_\kappa(\omega(\boldsymbol{g}\boldsymbol{g}_m^{-1}))$$

of non–negative radially symmetric kernels $\psi_\kappa(\omega(\circ\, \boldsymbol{g}_m^{-1}))$ centered at grid nodes $\boldsymbol{g}_m$ resulting in

$$\mathcal{X} f(\mathbf{h}, \mathbf{r}) = \sum_{m=1}^{M} c_m \left(\mathcal{R}\psi_\kappa(\boldsymbol{g}_m \mathbf{h}, \mathbf{r}) + \mathcal{R}\psi_\kappa(-\boldsymbol{g}_m \mathbf{h}, \mathbf{r}) \right)$$

modelling the diffraction pole intensities, where $\mathcal{R}$ denotes the Radon transform.

Resolution of the pdf–to–odf inversion problem

... and resolution of the inverse problem

Then the non–linear problem to be solved reads

$$\hat{\mathbf{c}} = \operatorname{argmin} \sum_{i=1}^{N} \sum_{j_i=1}^{N_i} \Big(\sum_{m=1}^{M} a(\mathbf{h}_i)\, c_m\, \mathcal{X}\psi_\kappa(\boldsymbol{g}_m \mathbf{h}_i, \mathbf{r}_{j_i}) + I^b_{ij_i} - \mathbf{I}_{ij_i} \Big)^2$$

$$+ \lambda \left\| \sum_{m=1}^{M} c_m\, \psi_\kappa(\circ\, \boldsymbol{g}_m^{-1}) \right\|^2_{\mathcal{H}(\mathrm{SO}(3))} ,$$

where λ is the parameter of regularization weighting the penalty term.

Kernel density estimation of individual orientation measurements

Kernel density estimator and its Radon transform

The odf is modelled as a positive linear combination

$$\widehat{f}_\kappa(\boldsymbol{g}; \boldsymbol{g}_1, \ldots, \boldsymbol{g}_n) = \frac{1}{n} \sum_{i=1}^{n} \psi_\kappa(\omega(\boldsymbol{g}\boldsymbol{g}_i^{-1}))$$

of non–negative radially symmetric kernels $\psi_\kappa(\omega(\circ\, \boldsymbol{g}_i^{-1}))$ centered at observed individual orientations $\boldsymbol{g}_i$ resulting in corresponding pdfs

$$\mathcal{X}[\widehat{f}_\kappa(\circ; \boldsymbol{g}_1, \ldots, \boldsymbol{g}_n)](\mathbf{h}, \mathbf{r}) = \frac{1}{n} \sum_{i=1}^{n} \Big(\mathcal{R}\psi_\kappa(\boldsymbol{g}_i \mathbf{h} \cdot \mathbf{r}) + \mathcal{R}\psi_\kappa(-\boldsymbol{g}_i \mathbf{h} \cdot \mathbf{r}) \Big) .$$

Estimation of $C_\ell^{kk'}$

Unbiased estimator $\widehat{C}_\ell^{kk'}$

$$\widehat{C}_\ell^{kk'}(\boldsymbol{g}_1, \ldots, \boldsymbol{g}_n) = \frac{1}{n} \sum_{i=1}^{n} T_\ell^{kk'}(\boldsymbol{g}_i), \;\; \ell = 1, \ldots, L$$

Estimation of $C_\ell^{kk'}$

Dirichlet kernel

$$\begin{aligned}
\psi_L(\omega(\boldsymbol{g}\boldsymbol{g}_0^{-1})) &= \sum_{\ell=0}^{L} \sum_{k,k'=-\ell}^{\ell} (2\ell+1)\, T_L^{kk'}(\boldsymbol{g})\, T_L^{kk'}(\boldsymbol{g}_0) \\
&= \sum_{\ell=0}^{L} (2\ell+1)\, \frac{\sin\left((2\ell+1)\frac{\omega(\boldsymbol{g}\boldsymbol{g}_0^{-1})}{2}\right)}{\sin\frac{\omega(\boldsymbol{g}\boldsymbol{g}_0^{-1})}{2}} \\
&= \sum_{\ell=0}^{L} (2\ell+1)\, \mathcal{U}_{2\ell}\left(\cos\frac{\omega(\boldsymbol{g}\boldsymbol{g}_0^{-1})}{2}\right)
\end{aligned}$$

spatial domain

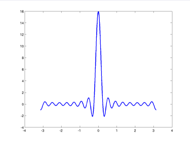

frequency domain

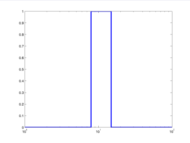

Estimation of $C_\ell^{kk'}$

Harmonic coefficients of Dirichlet kernel density estimator

With the Dirichlet kernel we get

$$\widehat{f}_{\mathcal{D}_L}(\boldsymbol{g};\boldsymbol{g}_1,\ldots,\boldsymbol{g}_n)=\frac{1}{n}\sum_{i=1}^{n}\sum_{\ell=0}^{L}(2\ell+1)\,\mathcal{U}_{2\ell}\left(\cos\frac{\omega(\boldsymbol{g}\boldsymbol{g}_i^{-1})}{2}\right)$$

with

$$C_\ell^{kk'}(\widehat{f}_{\mathcal{D}_L})=\begin{cases}\widehat{C}_\ell^{kk'}(\boldsymbol{g}_1,\ldots,\boldsymbol{g}_n), & \text{if } \ell\leq L\\ 0, & \text{otherwise}\end{cases}$$

which is the

Unbiased estimator $\widehat{C}_\ell^{kk'}$

$$\widehat{C}_\ell^{kk'}(\boldsymbol{g}_1,\ldots,\boldsymbol{g}_n)=\frac{1}{n}\sum_{i=1}^{n}T_\ell^{kk'}(\boldsymbol{g}_i),\;\;\ell=1,\ldots,L.$$

Simulated EBSD data

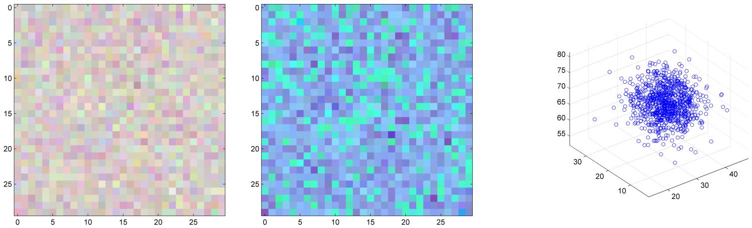

900 simulated spatially indexed individual orientations according to Bingham quaternion distribution

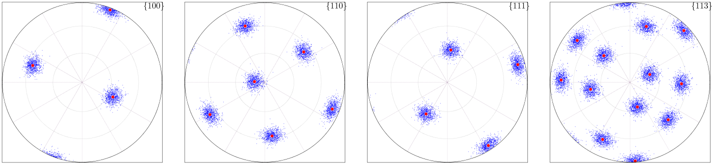

Pole point plots for crystal forms $\{100\}, \{110\}, \{111\}$, and $\{113\}$

Single crystal EBSD data (courtesy W. Pantleon, Risø)

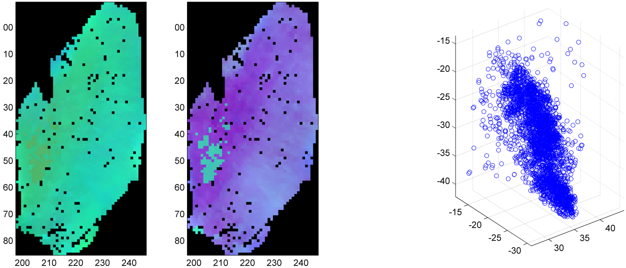

Grain 40 with 3068 spatially indexed individual orientations

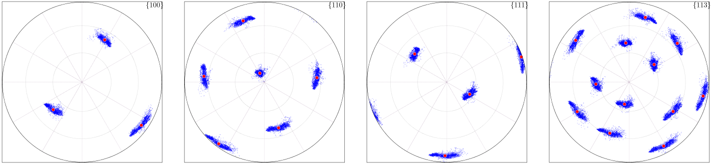

Pole point plots of grain 40 for crystal forms $\{100\}, \{110\}, \{111\}$, and $\{113\}$

Single crystal EBSD data (courtesy W. Pantleon, Risø)

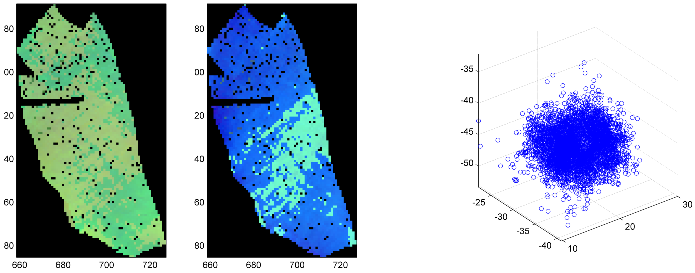

Grain 147 with 4324 spatially indexed individual orientations

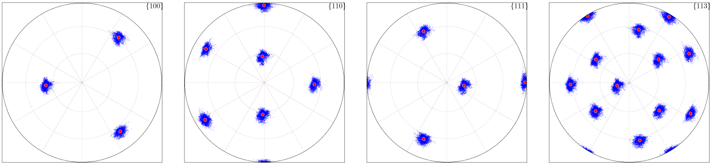

Pole point plots of grain 147 for crystal forms $\{100\}, \{110\}, \{111\}$, and $\{113\}$

Single crystal EBSD data (courtesy W. Pantleon, Risø)

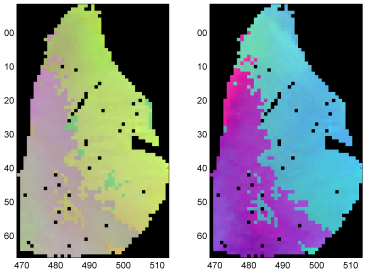

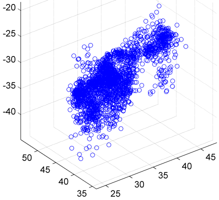

Grain 109 with 2253 spatially indexed individual orientations

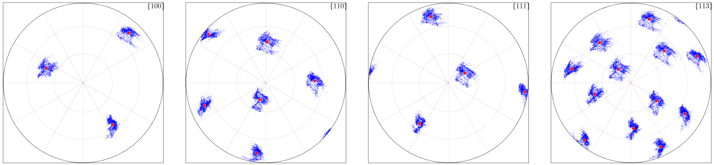

Pole point plots of grain 109 for crystal forms $\{100\}, \{110\}, \{111\}$, and $\{113\}$

Single crystal EBSD data (courtesy W. Pantleon, Risø)

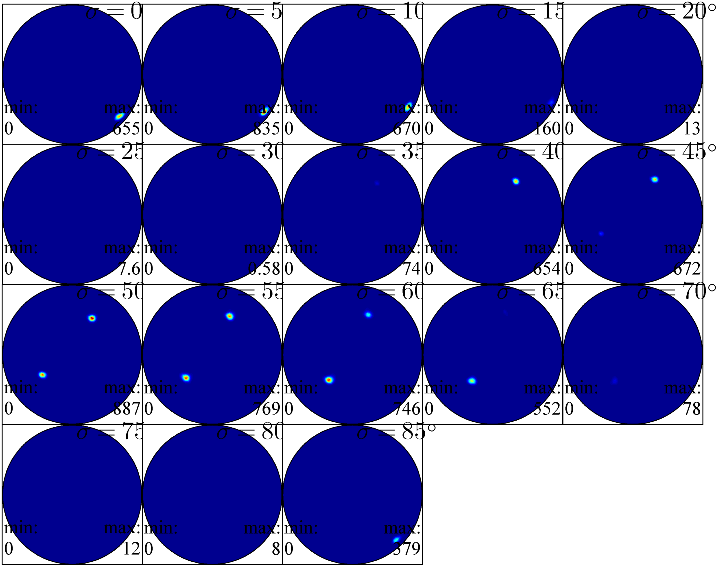

Single crystal EBSD data (courtesy W. Pantleon, Risø)

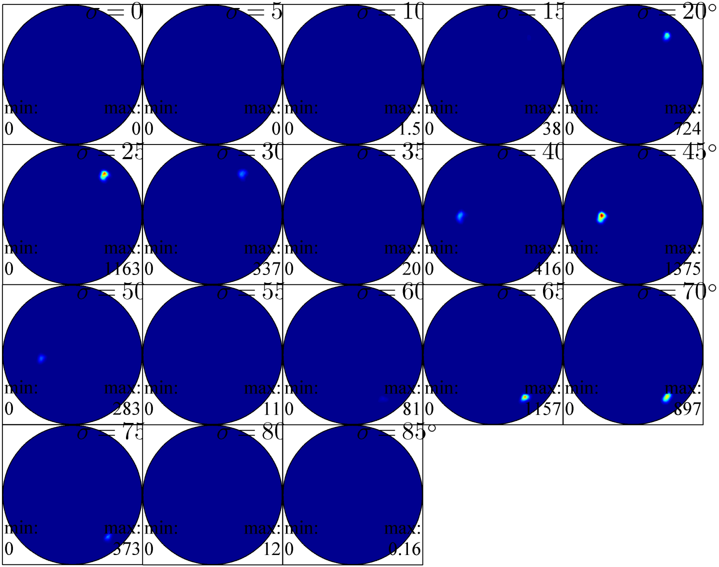

Single crystal EBSD data (courtesy W. Pantleon, Risø)

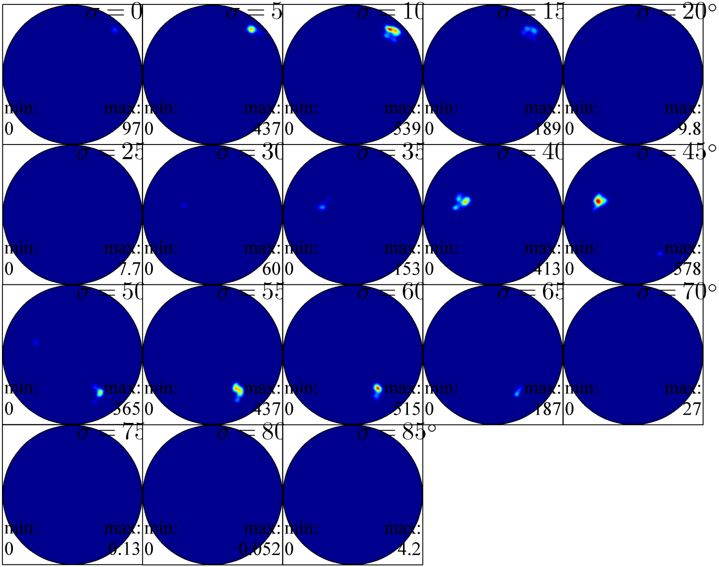

Single crystal EBSD data (courtesy W. Pantleon, Risø)

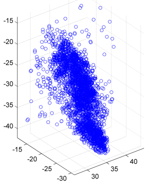

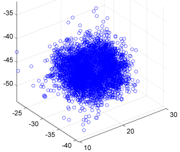

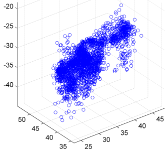

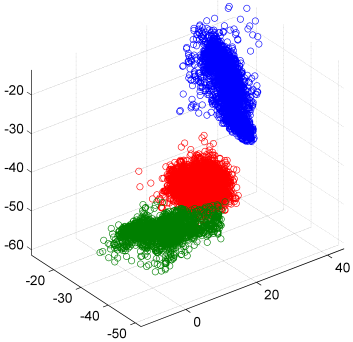

Statistics of EBSD data

The key statistics of orientation data is the "orientation tensor"

$$T = \frac{1}{n} \sum_{\ell=1}^{n} q_\ell q_\ell^\mathsf{T}$$

and its spectral decomposition, where the set of eigenvectors $a_1, \ldots, a_4$ provides a measure of location and the set of corresponding eigenvalues $\lambda_1, \ldots, \lambda_4$ provides a corresponding measure of dispersion. Since the orientation tensor T and the tensor of inertia I are related by

$$I = E - T$$

the eigenvectors of T provide the principal axes of inertia and the eigenvalues of T provide the principal moments of inertia.

In general, a single eigenvector and its eigenvalue do not provide a reasonable characterization of the data. Therefore, often the ratios of the eigenvalues are being analyzed and interpreted.

Statistics of EBSD data (courtesy W. Pantleon, Risø)

The spectral analyses of the orientation matrices T are numerically summarized in the following table.

	simIOM	grain 40	grain 147	grain 109
sample size	900	3068	4324	2253
texture index	61.2971	337.7395	308.9108	178.4238
entropy	-3.6491	-5.3425	-5.1136	-4.7782
λ_1	0.9954	0.9965	0.9983	0.9956
λ_2	0.0016	0.0029	0.0009	0.0022
λ_3	0.0015	0.0003	0.0005	0.0019
λ_4	0.0014	0.0003	0.0004	0.0003
λ_2/λ_3	1.1043	9.7599	1.7465	1.1364
λ_3/λ_4	1.0517	1.1345	1.4199	6.1100
interpretation by inspection	spherical	prolate	spherical	oblate

Conclusions: An Appreciation of Modern Numerics

Our novel approach matches the challenges and requirements of modern texture analysis to a large extent.

Conclusions: An Appreciation of Modern Numerics

Our novel approach matches the challenges and requirements of modern texture analysis to a large extent.

The method applies to

- any crystal symmetry, superpositions of crystal directions,
- arbitrarily scattered specimen directions, e.g., area detector data,
- high resolution or locally refined pole figure data,
- sharp textures,
- C–coefficients, volume portions, texture index, entropy, etc.

Conclusions: An Appreciation of Modern Numerics

Our novel approach matches the challenges and requirements of modern texture analysis to a large extent.

The method applies to

- any crystal symmetry, superpositions of crystal directions,
- arbitrarily scattered specimen directions, e.g., area detector data,
- high resolution or locally refined pole figure data,
- sharp textures,
- C–coefficients, volume portions, texture index, entropy, etc.

Unique approach to analyse integral and individual orientation measurements.

Matlab toolbox MTEX

MTEX Software

For the free and open–source Matlab toolbox MTEX see

http://code.google.com/p/mtex/

Accompanying publication

Hielscher, R., Schaeben, H., 2008,
A novel pole figure inversion method:
Specification of the MTEX algorithm:
Journal of Applied Crystallography 41, 1024-1037

The End

Thank you for your attention.

helmut.schaeben@geo.tu-freiberg.de